Inorganic Chemistry

Article

pubs.acs.org/IC

Expansion of the Hexagonal Phase-Forming Region of $Lu_{1-x}Sc_xFeO_3$ by Containerless Processing

Atsunobu Masuno,*[,†] Atsushi Ishimoto,[†] Chikako Moriyoshi,[‡] Hitoshi Kawaji,[§] Yoshihiro Kuroiwa,[‡] and Hiroyuki Inoue[†]

[†]Institute of Industrial Science, The University of Tokyo, Meguro-ku, Tokyo 153-8505, Japan

[‡]Department of Physical Science, Hiroshima University, Higashi-Hiroshima, Hiroshima 739-8526, Japan

[§]Materials & Structures Laboratory, Tokyo Institute of Technology, Midori-ku, Yokohama 226-8503, Japan

Supporting Information

ABSTRACT: Hexagonal $Lu_{1-x}Sc_xFeO_3$ ($0 \leq x \leq 0.8$) was directly solidified from an undercooled melt by containerless processing with an aerodynamic levitation furnace. The hexagonal phase-forming region was considerably extended compared to that of the conventional solid-state reaction ($x \sim 0.5$). Synchrotron X-ray diffraction measurements revealed that the crystal structure of the hexagonal phase was isomorphous to hexagonal ferroelectric $RMnO_3$ (R = a rare earth ion) with a polar space group of $P6_3cm$. As x increased, the a-axis lattice constant decreased linearly, strengthening the antiferromagnetic interaction between the Fe^{3+} ions on the $a-b$ plane. Accordingly, the weak ferromagnetic transition temperature increased from 150 K for $x = 0$ to 175 K for $x = 0.7$. These transition temperatures were much higher than those of hexagonal $Lu_{1-x}Sc_xMnO_3$. The results indicate that hexagonal $Lu_{1-x}Sc_xFeO_3$ is a suitable alternative magnetic dielectric for use at higher temperatures.

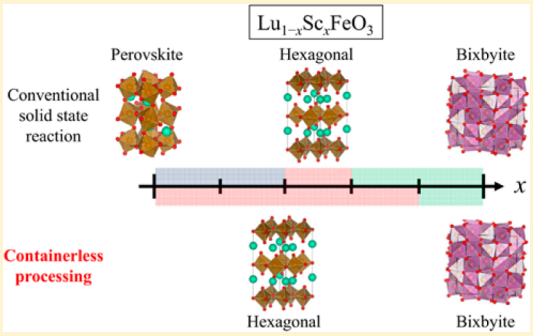

INTRODUCTION

The phase stability of the perovskite structure for RMO_3 compounds (R^{3+} = a rare earth ion, and M = a trivalent transition metal ion) decreases with a decreasing ionic radius of R^{3+}. The tolerance factor t, which depends on the ionic radii of components, is generally used to evaluate the stability quantitatively.[1] When M = Mn^{3+} and the ionic radius of R^{3+} is smaller than that of Ho^{3+}, the hexagonal structure is more stable than the perovskite structure.[2−4] Hexagonal $RMnO_3$ (h-$RMnO_3$) has attracted much attention because of its fascinating combination of magnetic, ferroelectric, and elastic properties.[5−10] Conversely, because the difference in stability between the perovskite and hexagonal phases is not large, even when the ionic radius of R is very small, perovskite $RMnO_3$ can be obtained as a metastable phase by high-pressure synthesis or thin-film growth techniques.[2,3]

For M = Fe^{3+}, the perovskite structure is much more stable than it is for $RMnO_3$ compounds, although the ionic radii of Fe^{3+} and Mn^{3+} are almost identical. $RFeO_3$ has a perovskite structure for R = all rare earth ions except for Sc^{3+}. However, similar to that of $RMnO_3$, the phase stability of $RFeO_3$ can be adjusted by metastable formation techniques. Metastable hexagonal $RFeO_3$ (h-$RFeO_3$) has been prepared as bulk powder crystallized from amorphous precursors[11−15] or levitated melts[16,17] and as thin films.[18−28] h-$RFeO_3$ exhibits interesting properties similar to those of h-$RMnO_3$ and some properties that are even more desirable. The weak ferromagnetic transition temperature T_N of h-$RFeO_3$ thin films depends strongly on the ionic radius of R^{3+}, the degree of lattice strain induced by the substrates, and the quality of the films. Nevertheless, the T_N of h-$RFeO_3$ thin films is in the range of 100−150 K, which is higher than those of h-$RMnO_3$ with the same R ion. The high magnetic transition temperature was explained by the larger magnetic interaction on the $a-b$ plane, because the a-axis length was shorter than that of h-$RMnO_3$ and the spin magnetic moment of Fe^{3+} ($S = {}^5/_2$) was larger than that of Mn^{3+} ($S = 2$). The ferroelectricity of h-$RFeO_3$ thin films at room temperature was confirmed by the polarization-field hysteresis loop.[21,23] The ferroelectric ordering and domain walls were directly observed by scanning transmission electron microscopy[26] as in the case of h-$RMnO_3$.[29] Therefore, h-$RFeO_3$ compounds are considered to be suitable alternative multiferroic materials for use at higher temperatures as compared with h-$RMnO_3$.[30]

For R = Sc^{3+}, which has an ionic radius smaller than that of Lu^{3+}, the perovskite structure is no more stable. However, the stable phase for $ScFeO_3$ is bixbyite instead of hexagonal.[31] Recently, we have found that a stable hexagonal phase can be obtained in a very narrow composition region in $Lu_{1-x}Sc_xFeO_3$ by a conventional solid-state reaction.[32] The stable region of the hexagonal phase is $x \sim 0.5$, which is located between the

Received: May 30, 2015
Published: September 17, 2015

DOI: 10.1021/acs.inorgchem.5b01225
Inorg. Chem. 2015, 54, 9432−9437

stable regions of the perovskite and bixbyite phases. This means that decreasing the average ionic radii of R^{3+} changes the stable structure of $RFeO_3$ sequentially from perovskite to hexagonal and then to the bixbyite structure. The weak ferromagnetic transition temperature of hexagonal $Lu_{0.5}Sc_{0.5}FeO_3$ was at 162 K with a dielectric anomaly, which is the highest temperature observed for *h*-$RFeO_3$ and *h*-$RMnO_3$ compounds. Hexagonal $Lu_{0.5}Sc_{0.5}FeO_3$ is stable, meaning that hexagonal $Lu_{1-x}Sc_xFeO_3$ can be obtained over a wide range of compositions around $x \sim 0.5$ by metastable formation techniques. Previously, we reported that containerless processing could stabilize hexagonal $LuFeO_3$ solidified directly from an undercooled melt.[16,17] Therefore, in this study, containerless processing is applied to $Lu_{1-x}Sc_xFeO_3$ ($0 \le x \le 1$) to obtain a hexagonal phase over a wide composition range, although the stability of the hexagonal and bixbyite phases is still unclear. The crystal structure and magnetic properties of hexagonal $Lu_{1-x}Sc_xFeO_3$ are also investigated.

EXPERIMENTAL SECTION

High-purity Lu_2O_3, Sc_2O_3, and Fe_2O_3 powders were mixed in chemical compositions of $Lu_{1-x}Sc_xFe_{1.2}O_3$ ($0 \le x \le 1$). The extra 20 mol % of iron oxide was necessary to obtain stoichiometric $Lu_{1-x}Sc_xFeO_3$, because iron oxides often evaporate during containerless processing.[16] The mixed powders were pelletized and sintered at 1000 °C for 12 h in air. A piece of the pellets (~10 mg) was melted in an aerodynamic levitation (ADL) furnace. Oxygen gas was used to levitate a melt. A 100 W CO_2 laser was used to melt the levitated sample. The details of the ADL furnace are described elsewhere.[16,17] The sample was kept above the melting point for ~10 s to ensure that the melt was homogenized. After homogeneous melting of the sample, the laser power was turned off and the sample was rapidly cooled to room temperature at a rate of hundreds of kelvins per second. Crystallization occurred after the melt was undercooled below the melting temperature. The crystallization was clearly observed as light emission caused by the release of the latent heat from the undercooled melt, known as recalescence. Chemical composition analyses for the as-solidified samples were conducted by an energy dispersive X-ray fluorescence spectrometer. There were almost no chemical deviations in the Lu and Sc ratio from the starting materials. Although the excess of iron of the solidified samples was smaller than those of the starting materials, there were still an excess of iron oxides of approximately 10 mol %. It seems that the (Lu + Sc):Fe ratio was not unique to each sample, which may cause difficulty for the refinement of crystal structure parameters in crystal structure analysis.

For crystal structure analysis of the solidified samples, the high-energy synchrotron radiation (SR) X-ray powder diffraction measurements were performed at room temperature with a large Debye–Scherrer camera installed at BL02B2 in SPring-8.[33] The sample was ground in an agate mortar and sealed in a quartz capillary with an internal diameter of 0.1 mm. The SR wavelength was $\lambda = 0.49608(7)$ Å. The crystal structures were analyzed by the Rietveld method with the diffraction intensity data up to 2θ of 45° ($d > 0.65$ Å). Before the magnetic properties of compounds with a hexagonal structure were measured, magnetic impurities, such as Fe_3O_4, were removed by the magnetic separation method. After the as-solidified samples had been crushed, they were dispersed in the acetone in a beaker. When a magnet was added to the beaker, the impurities having magnetization at room temperature attached to the magnet. After the magnet was removed from the beaker, we obtained purified samples. The temperature dependence of the magnetic moment was measured in a temperature range of 5–300 K at a magnetic field of 1000 Oe using a superconducting quantum interference device magnetometer (SQUID, MPMS, Quantum Design Inc., San Diego, CA).

RESULTS AND DISCUSSION

Figure 1 shows the synchrotron XRD profiles of samples solidified from undercooled melts. The peaks from the

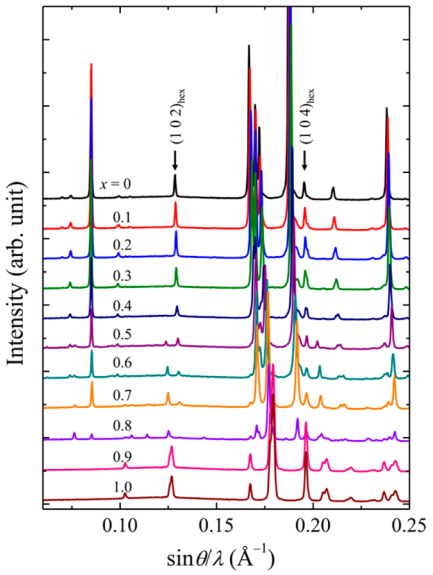

Figure 1. Synchrotron X-ray diffraction profiles of $Lu_{1-x}Sc_xFeO_3$ solidified from an undercooled melt by containerless processing. $\lambda = 0.49608(7)$ Å. The arrows show the weak reflection peaks allowed in the noncentrosymmetric $P6_3cm$ space group.

hexagonal phase were observed in the range of $0 \le x \le 0.8$, which is considerably larger than the range for the conventional solid-state reaction. The crystal structures of the $x = 0$–0.8 compounds are isomorphous to *h*-$RMnO_3$. The intensities of the peak characteristics of the hexagonal phase at $\sin\theta/\lambda = 0.13$ and 0.19 decrease from $x = 0$ to $x = 0.8$. Those weak peaks originate from (1 0 2) and (1 0 4) reflections, respectively, which are allowed in the noncentrosymmetric $P6_3cm$ space group. The peaks originating from the bixbyite phase increase from $x = 0.6$ to $x = 1.0$. At approximately $x = 0.8$, Fe_3O_4 solidified as an impurity phase distinct from the hexagonal and bixbyite phases.

The mole fractions of the perovskite and bixbyite phase were estimated by the Rietveld analysis after impurities such as Fe_3O_4 were subtracted from the data. Figure 2 shows the composition dependence of the mole fraction of the hexagonal and bixbyite phases. The fraction of the hexagonal phase is 100% when x is smaller than 0.5, whereas it decreases for $x >$

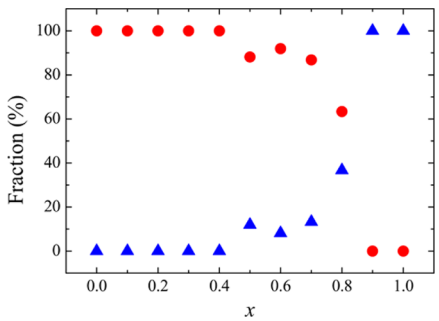

Figure 2. Mole fraction of the hexagonal (circles) and bixbyite (triangles) phases as a function of x in $Lu_{1-x}Sc_xFeO_3$ solidified from an undercooled melt.

DOI: 10.1021/acs.inorgchem.5b01225
Inorg. Chem. 2015, 54, 9432–9437

0.5 in the region where the bixbyite phase is stable for solid-state synthesis. These results indicate that because the bixbyite structure is stable and crystallizes easily, metastable phases, such as the hexagonal phase, cannot be obtained even though the melt is undercooled. The composition limit of hexagonal $Lu_{1-x}Sc_xFeO_3$ is $x = 0.8$ for containerless processing.

Figure 3 shows the composition dependence of the lattice parameters and the unit cell volume of hexagonal $Lu_{1-x}Sc_xFeO_3$

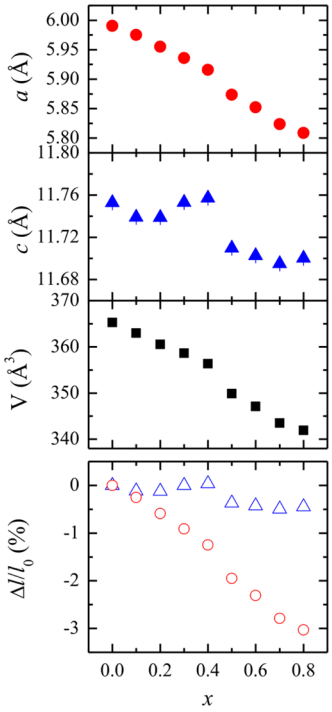

Figure 3. Composition dependence of *a*-axis and *c*-axis lattice parameters, the volume, and the ratio of the change in the lattice parameter $\Delta l/l$ of hexagonal $Lu_{1-x}Sc_xFeO_3$. $\Delta l/l$ is calculated from the equation $(l_x - l_0)/l_0$, where l_0 corresponds to the lattice parameters a_0 and c_0 of *h*-$LuFeO_3$ and l_x corresponds to those of $Lu_{1-x}Sc_xFeO_3$.

$(0 \le x \le 0.8)$. The lattice parameters and the reliability factors for the results of the Rietveld analysis are given in the Supporting Information. The lattice parameters monotonically decrease as x increases. The lattice parameters of the $x = 0.5$ compound are in good agreement with those of $Lu_{0.5}Sc_{0.5}FeO_3$ obtained by the conventional solid-state reaction,[32] which indicates that at $x = 0.5$, the same material is produced by both processes. Volume V gradually decreases as x increases, suggesting that the Sc^{3+} ion, which has an ionic radius smaller than that of Lu^{3+}, is substituted into the Lu^{3+} sites.

To clarify the composition dependence of the lattice parameters further, the ratios of the changes in the lattice parameter $\Delta l/l$ are also shown in Figure 3. $\Delta l/l$ is calculated from the equation $(l_x - l_0)/l_0$, where l_0 corresponds to lattice parameters a_0 and c_0 of *h*-$LuFeO_3$ and l_x corresponds to those of $Lu_{1-x}Sc_xFeO_3$. The change in lattice parameter *a* is greater than that of lattice parameter *c*. The lattice parameter change of the *a*-axis is −3.0% at $x = 0.8$, whereas that of the *c*-axis is at most −0.4%. This anisotropic behavior was observed in the Mn oxide system. For example, in the case of hexagonal $Lu_{1-x}Sc_xMnO_3$, when x increases from 0 to 1, the changes in the *a*-axis and *c*-axis lengths are −3.6 and −1.8%, respectively.[34] Via comparison of *h*-$YMnO_3$ and *h*-$LuMnO_3$, the changes in the *a*-axis and *c*-axis lengths from Y^{3+} to Lu^{3+} are −1.6 and −0.3%, respectively.[35] The anisotropy of *h*-RMO_3 (M = Mn^{3+} or Fe^{3+}) can be explained by simultaneous displacement of atoms caused by substituting R^{3+}. Figure 4 shows the schematic

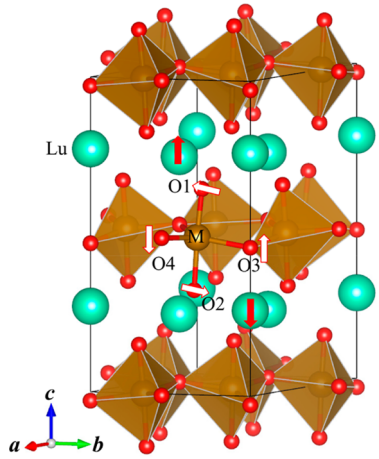

Figure 4. Schematic illustration of the crystal structure of hexagonal RMO_3 (M = Mn^{3+} or Fe^{3+}). Arrows indicate the displacement of atoms upon substitution of the smaller R^{3+} ion.

illustration of the crystal structure of *h*-RMO_3. The hexagonal structure comprises closely packed layers of trigonal MO_5 bipyramids, where each M^{3+} ion is surrounded by three in-plane and two apical O^{2-} ions. The MO_5 bipyramids share the in-plane oxygen ions to form a triangular lattice in the *a*−*b* plane, and they are separated along the *c*-axis by R layers. When R is substituted with a smaller one, the tilting of the MO_5 bipyramids will be caused by the displacement of the apical oxygen (O1 and O2) along the *a*−*b* plane, which pushes off R along the *c*-axis. The tilting of MO_5 leads to the displacement of the in-plane oxygen (O3 and O4); however, the two oxygens move in the opposite direction along the *c*-axis, and then buckling of the R layers should occur.[35] As a result, the change in the *c*-axis lattice constant is suppressed compared to that of the *a*-axis lattice constant, causing the anisotropy. Comparing the atomic coordinates of *h*-$LuFeO_3$ and *h*-$Lu_{0.5}Sc_{0.5}FeO_3$ reported in the previous works[17,32] supports the anisotropic effect of the average size of R on the unit cell. The volume of Lu−O_7 polyhedra is 16.8323 Å^3, and the averaged Lu−O distance is 2.256 Å in *h*-$LuFeO_3$. The volume of Lu/Sc−O_7 polyhedra is 15.6180 Å^3, and the averaged Lu/Sc−O distance is 2.214 Å in *h*-$Lu_{0.5}Sc_{0.5}FeO_3$. The shrinkage is explained by the small ionic radius of Sc compared to that of Lu. Furthermore, by substitution of Sc, the Lu/Sc1−O3 distance becomes larger than the Lu1−O3 distance and the angle between the O1−O2 bond and *c*-axis decreases. Accordingly, the tilting of FeO_5 polyhedra is relaxed by substitution of Sc, and then the decrease in the *c*-axis lattice constant is suppressed compared to that of the *a*-axis.

Furthermore, it is noted that the anisotropy of the lattice constant change of *h*-$RFeO_3$ is much larger than that of *h*-$RMnO_3$. This is caused by the different electronic configuration between Mn^{3+} (d^4) and Fe^{3+} (d^5) in the MO_5 bipyramid. The z^2 orbital of the FeO_5 bipyramid is occupied by one electron as the highest occupied orbital, while it is empty in the MnO_5 bipyramid.[18] The additional occupied orbital of the FeO_5 bipyramid causes the great repulsion between the electron and the apical oxygen along the *c*-axis. Accordingly, the

DOI: 10.1021/acs.inorgchem.5b01225
Inorg. Chem. 2015, 54, 9432−9437

suppression of change in the *c*-axis of *h*-$RFeO_3$ accompanied by the tilting of the FeO_5 bipyramid is larger than that of *h*-$RMnO_3$.

The temperature dependence of the molar magnetic susceptibility at 1000 Oe in the zero-field-cooled (ZFC) or the field-cooled (FC) mode of hexagonal $Lu_{1-x}Sc_xFeO_3$ ($0 \leq x \leq 0.7$) is shown in Figure 5. Although the careful purification

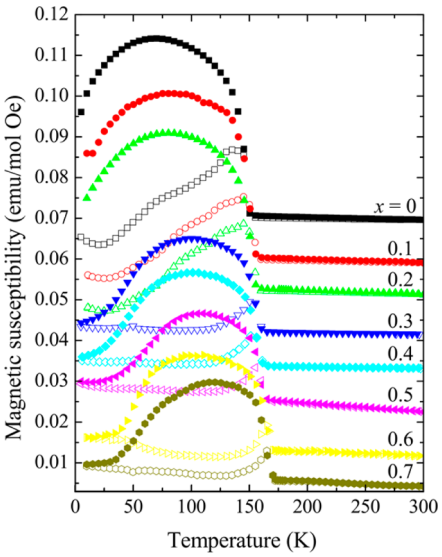

Figure 5. Temperature dependence of the magnetic susceptibility of hexagonal $Lu_{1-x}Sc_xFeO_3$ at 1 kOe. Filled and empty symbols represent FC and ZFC, respectively.

for magnetic impurities in the as-solidified samples was conducted, Fe_3O_4 often remained. The $x = 0.5$ and 0.7 curves had a slope at high temperatures larger than those of others because Fe_3O_4 was still a magnetic impurity. The $x \geq 0.5$ samples would contain a small amount of impurities of the bixbyite phase as shown in Figure 2. However, the magnetic susceptibility of the bixbyite phase should be negligible because the magnetic susceptibility of the bixbyite $ScFeO_3$ was considerably small compared to that of the hexagonal phase.[31] The small magnetization at low temperatures indicates that the magnetic interaction is antiferromagnetic. The magnetic transition temperature was defined as the temperature at which both the ZFC and FC curves show a rapid increase. To estimate the Weiss temperature, the magnetic susceptibility data in the paramagnetic region were fitted to the Curie–Weiss formula. However, unfortunately, the Weiss temperatures were dispersed in the vicinity of −1000 K for each composition, and it was difficult to determine the composition dependence of the temperature. The large dispersion may be caused by the magnetic impurities. In the case of *h*-$Lu_{0.5}Sc_{0.5}FeO_3$, the Weiss temperature was reported to be approximately −600 K in our previous work.[32] Therefore, it can be concluded that the Weiss temperatures were negative even though it was difficult to obtain absolute values of the Weiss temperature because of magnetic impurities. In this study, we focused on the composition dependence of the magnetic transition temperature. The magnetic transition temperature, T_N, of *h*-$LuFeO_3$ was 150 K, although the T_N of *h*-$LuFeO_3$ thin films varied from 120 to 150 K.[22−24,26,28] Figure 6 shows the composition dependence of T_N. T_N decreases linearly with an increasing x to 175 K at $x = 0.7$. As shown in the inset of Figure 6, T_N increases

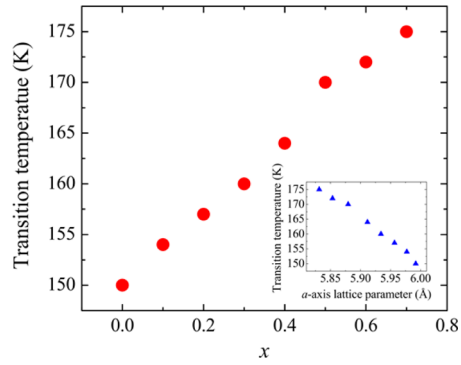

Figure 6. Composition dependence of the magnetic transition temperature of hexagonal $Lu_{1-x}Sc_xFeO_3$. The inset shows the *a*-axis lattice parameter dependence of T_N.

linearly with an increase in the *a*-axis length, indicating that the increase in T_N is caused by the increase in the extent of the magnetic interaction arising from the decreasing Fe–O bond length on the *a*–*b* plane. The linear increase in T_N caused by substituting Sc^{3+} for Lu^{3+} is similar to that reported in the *h*-$Lu_{1-x}Sc_xMnO_3$ solid solution system, which shows an increase from 92 to 133 K.[34] However, the values of T_N for *h*-$Lu_{1-x}Sc_xFeO_3$ are much higher than those for *h*-$Lu_{1-x}Sc_xMnO_3$, indicating that the magnetic interaction in *h*-$Lu_{1-x}Sc_xFeO_3$ is much larger. This is because the strength of the exchange interaction in the *a*–*b* plane between Fe^{3+}, which has one more unpaired electron than Mn^{3+}, is larger than that between Mn^{3+}.[36−38] Increasing the transition temperature in the $Lu_{1-x}Sc_xFeO_3$ system further may be impossible because the stable bixbyite phase at larger x prevents the formation of the hexagonal phase.

The temperature dependence of the magnetic moment of *h*-$Lu_{1-x}Sc_xFeO_3$ exhibited further interesting properties. For the $x = 0$ compound, the magnetization increases as the temperature decreases below T_N, and in the FC curve, the value decreases at a lower temperature. However, the magnetization does not match that of the ZFC curve at the lowest temperature, indicating that a spin canting remains. Weak ferromagnetic properties have also been reported in *h*-$LuFeO_3$ thin films. The DFT calculations suggested that the Fe^{3+} spins in the ground state form a 120° triangular spin structure on the *a*–*b* plane, resulting in a zero residual moment along the *a*–*b* plane, whereas the Fe^{3+} spins are slightly canted with a non-zero moment along the *c*-axis.[23] Therefore, although the magnetic structure of bulk *h*-$LuFeO_3$ is still unclear, the distinctive weak ferromagnetic behavior at the lowest temperature supports the suggestion that the Fe^{3+} spins align in a 120° triangular spin structure in the *a*–*b* plane, although they are canted along the *c*-axis. The difference in magnetization between FC and ZFC at the lowest temperature decreases as x increases. At $x \geq 0.3$, there is almost no difference between them, and the suppression of the FC curve at low temperatures occurred at higher temperatures as x increased, indicating that the extent of antiferromagnetic interaction in the *a*–*b* plane increases and preventing the Fe^{3+} spins from canting along the *c*-axis.

The ZFC curve of *h*-$LuFeO_3$ shows a gradual increase in magnetization around 30 K, and a further increase is observed at 80 K. These increases may be caused by the spin reorientation, which was also observed in hexagonal $YMnO_3$, $LuMnO_3$, and $ScMnO_3$.[34] The complicated magnetic phase transition might also occur in hexagonal $LuFeO_3$. However, the

DOI: 10.1021/acs.inorgchem.5b01225
Inorg. Chem. 2015, 54, 9432–9437

spin reorientation temperature appears to increase as x increases. This may be caused by the decrease in the ferromagnetic component causing the complicated spin reorientation.

CONCLUSIONS

Hexagonal phases of $Lu_{1-x}Sc_xFeO_3$ were prepared by containerless processing. The hexagonal phase-forming region was expanded from $x = 0$ to $x = 0.8$. The lattice parameters decreased linearly as x increased. The a-axis length decreased more than the c-axis length. T_N increased with x depending on the a-axis length because of the stronger magnetic interaction on the $a-b$ plane. The T_N of 175 K for $Lu_{1-x}Sc_xFeO_3$ at $x = 0.7$ was the highest among those of the hexagonal iron and manganese oxides. This was achieved by the decrease in lattice parameter a caused by substituting Sc^{3+} for Lu^{3+} and the increase in the extent of the exchange interaction upon substitution of Fe^{3+} for Mn^{3+}. Hexagonal iron oxides are promising alternative materials to manganese oxides for high-temperature magnetic dielectrics.

ASSOCIATED CONTENT

Supporting Information

The Supporting Information is available free of charge on the ACS Publications website at DOI: 10.1021/acs.inorgchem.5b01225.

Additional information about the Rietveld analysis (PDF)

AUTHOR INFORMATION

Corresponding Author

*E-mail: masuno@iis.u-tokyo.ac.jp.

Notes

The authors declare no competing financial interest.

ACKNOWLEDGMENTS

The SR experiments were performed with the approval of the Japan Synchrotron Radiation Research Institute (JASRI; Proposals 2008B1040, 2010A1220, and 2013B1136). This research was partly supported by the Collaborative Research Project of Materials and Structures Laboratory, Tokyo Institute of Technology.

REFERENCES

(1) Zhou, J.-S.; Goodenough, J. B. *Phys. Rev. Lett.* **2014**, *94*, 065501.
(2) Zhou, J.-S.; Goodenough, J. B.; Gallardo-Amores, J. M.; Morán, E.; Alario-Franco, M. A.; Caudillo, R. *Phys. Rev. B: Condens. Matter Mater. Phys.* **2006**, *74*, 014422.
(3) Uusi-Esko, K.; Malm, J.; Imamura, N.; Yamauchi, H.; Karppinen, M. *Mater. Chem. Phys.* **2008**, *112*, 1029−1034.
(4) Ren, C.-Y. *Phys. Rev. B: Condens. Matter Mater. Phys.* **2009**, *79*, 125113.
(5) Katsufuji, T.; Mori, S.; Masaki, M.; Moritomo, Y.; Yamamoto, N.; Takagi, H. *Phys. Rev. B: Condens. Matter Mater. Phys.* **2001**, *64*, 104419.
(6) Van Aken, B. B.; Palstra, T. T. M.; Filippetti, A.; Spaldin, N. A. *Nat. Mater.* **2004**, *3*, 164−170.
(7) Lottermoser, T.; Lonkai, T.; Amann, U.; Hohlwein, D.; Ihringer, J.; Fiebig, M. *Nature* **2004**, *430*, 541−544.
(8) Cho, D.-Y.; Kim, J.-Y.; Park, B.-G.; Rho, K.-J.; Park, J.-H.; Noh, H.-J.; Kim, B. J.; Oh, S.-J.; Park, H.-M.; Ahn, J.-S.; Ishibashi, H.; Cheong, S.-W.; Lee, J. H.; Murugavel, P.; Noh, T. W.; Tanaka, A.; Jo, T. *Phys. Rev. Lett.* **2007**, *98*, 217601.
(9) Lee, S.; Pirogov, A.; Kang, M.; Jang, K.-H.; Yonemura, M.; Kamiyama, T.; Cheong, S.-W.; Gozzo, F.; Shin, N.; Kimura, H.; Noda, Y.; Park, J.-G. *Nature* **2008**, *451*, 805−808.
(10) Singh, S. K.; Patnaik, S.; Kaushik, S. D.; Siruguri, V. *Phys. Rev. B: Condens. Matter Mater. Phys.* **2010**, *81*, 184406.
(11) Yamaguchi, O.; Takemura, H.; Yamashita, M.; Hayashida, A. *J. Electrochem. Soc.* **1991**, *138*, 1492−1494.
(12) Mizoguchi, Y.; Onodera, H.; Yamauchi, H.; Kagawa, M.; Syono, Y.; Hirai, T. *Mater. Sci. Eng., A* **1996**, *217−218*, 164−166.
(13) Li, J.; Singh, U. G.; Schladt, T. D.; Stalick, J. K.; Scott, S. L.; Seshadri, R. *Chem. Mater.* **2008**, *20*, 6567−6576.
(14) Downie, L. J.; Goff, R. J.; Kockelmann, W.; Forder, S. D.; Parker, J. E.; Morrison, F. D.; Lightfoot, P. *J. Solid State Chem.* **2012**, *190*, 52−60.
(15) Nishimura, T.; Hosokawa, S.; Masuda, Y.; Wada, K.; Inoue, M. *J. Solid State Chem.* **2013**, *197*, 402−407.
(16) Masuno, A.; Sakai, S.; Arai, Y.; Tomioka, H.; Otsubo, F.; Inoue, H.; Moriyoshi, C.; Kuroiwa, Y.; Yu, J. *Ferroelectrics* **2009**, *378*, 169−174.
(17) Magome, E.; Moriyoshi, C.; Kuroiwa, Y.; Masuno, A.; Inoue, H. *Jpn. J. Appl. Phys.* **2010**, *49*, 09ME06.
(18) Bossak, A. A.; Graboy, I. E.; Gorbenko, O. Y.; Kaul, A. R.; Kartavtseva, M. S.; Svetchnikov, V. L.; Zandbergen, H. W. *Chem. Mater.* **2004**, *16*, 1751−1755.
(19) Akbashev, A. R.; Semisalova, A. S.; Perov, N. S.; Kaul, A. R. *Appl. Phys. Lett.* **2011**, *99*, 122502.
(20) Iida, H.; Koizumi, T.; Uesu, Y.; Kohn, K.; Ikeda, N.; Mori, S.; Haumont, R.; Janolin, P.-E.; Kiat, J.-M.; Fukunaga, M.; Noda, Y. *J. Phys. Soc. Jpn.* **2012**, *81*, 024719.
(21) Jeong, Y. K.; Lee, J.-H.; Ahn, S.-J.; Song, S.-W.; Jang, H. M.; Choi, H.; Scott, J. F. *J. Am. Chem. Soc.* **2012**, *134*, 1450−1453.
(22) Wang, W.; Wang, H.; Xu, X.; Zhu, L.; He, L.; Wills, E.; Cheng, X.; Keavney, D. J.; Shen, J.; Wu, X.; Xu, X. *Appl. Phys. Lett.* **2012**, *101*, 241907.
(23) Jeong, Y. K.; Lee, J.-H.; Ahn, S.-J.; Jang, H. M. *Chem. Mater.* **2012**, *24*, 2426−2428.
(24) Pavlov, V. V.; Akbashev, A. R.; Kalashnikova, A. M.; Rusakov, V. A.; Kaul, A. R.; Bayer, M.; Pisarev, R. V. *J. Appl. Phys.* **2012**, *111*, 056105.
(25) Ahn, S.-J.; Lee, J.-H.; Jeong, Y. K.; Na, E.-H.; Koo, Y. M.; Jang, H. M. *Mater. Chem. Phys.* **2013**, *138*, 929−936.
(26) Roddatis, V. V.; Akbashev, A. R.; Lopatin, S.; Kaul, A. R. *Appl. Phys. Lett.* **2013**, *103*, 112907.
(27) Ahn, S.-J.; Lee, J.-H.; Jang, H. M.; Jeong, Y. K. *J. Mater. Chem. C* **2014**, *2*, 4521−4525.
(28) Moyer, J. A.; Misra, R.; Mundy, J. A.; Brooks, C. M.; Heron, J. T.; Muller, D. A.; Schlom, D. G.; Schiffer, P. *APL Mater.* **2014**, *2*, 012106.
(29) Zhang, Q. H.; Wang, L. J.; Wei, X. K.; Yu, R. C.; Gu, L.; Hirata, A.; Chen, M. W.; Jin, C. Q.; Yao, Y.; Wang, Y. G.; Duan, X. F. *Phys. Rev. B: Condens. Matter Mater. Phys.* **2012**, *85*, 020102(R).
(30) Das, H.; Wysocki, A. L.; Geng, Y.; Wu, W.; Fennie, C. J. *Nat. Commun.* **2014**, *5*, 2998.
(31) Bréard, Y.; Fjellvåg, H.; Hauback, B. *Solid State Commun.* **2011**, *151*, 223−226.
(32) Masuno, A.; Ishimoto, A.; Moriyoshi, C.; Hayashi, N.; Kawaji, H.; Kuroiwa, Y.; Inoue, H. *Inorg. Chem.* **2013**, *52*, 11889−11894.
(33) Nishibori, E.; Takata, M.; Kato, K.; Sakata, M.; Kubota, Y.; Aoyagi, S.; Kuroiwa, Y.; Yamakata, M.; Ikeda, N. *Nucl. Instrum. Methods Phys. Res., Sect. A* **2001**, *467−468*, 1045−1048.
(34) Wu, C. T.; Lin, B. N.; Ku, H. C.; Hsu, Y. Y. *Chin. J. Phys.* **2003**, *41*, 652−660.
(35) Katsufuji, T.; Masaki, M.; Machida, A.; Moritomo, M.; Kato, K.; Nishibori, E.; Takata, M.; Sakata, M.; Ohoyama, K.; Kitazawa, K.; Takagi, H. *Phys. Rev. B: Condens. Matter Mater. Phys.* **2002**, *66*, 134434.
(36) Tomuta, D. G.; Ramakrishnan, S.; Nieuwenhuys, G. J.; Mydosh, J. A. *J. Phys.: Condens. Matter* **2001**, *13*, 4543−4552.

DOI: 10.1021/acs.inorgchem.5b01225
Inorg. Chem. 2015, 54, 9432−9437

(37) Park, J.; Lee, S.; Kang, M.; Jang, K.-H.; Lee, C.; Streltsov, S. V.; Mazurenko, V. V.; Valentyuk, M. V.; Medvedeva, J. E.; Kamiyama, T.; Park, J.-G. *Phys. Rev. B: Condens. Matter Mater. Phys.* **2010**, *82*, 054428.
(38) Samal, S. L.; Green, W.; Lofland, S. E.; Ramanujachary, K. V.; Das, D.; Ganguli, A. K. *J. Solid State Chem.* **2008**, *181*, 61−66.

DOI: 10.1021/acs.inorgchem.5b01225
Inorg. Chem. 2015, 54, 9432−9437